Fatigue crack propagation in composite laminates by a novel approach based on the S-N diagrams

Raimondo, Antonio; Bisagni, Chiara

Publication date
2019

Document Version
Accepted author manuscript

Published in
Proceedings of 22nd International Conference on Composite Materials (ICCM22), Melbourne, AU, August 11-16, 2019

FATIGUE CRACK PROPAGATION IN COMPOSITE LAMINATES BY A NOVEL APPROACH BASED ON THE S-N DIAGRAMS

A. Raimondo and C. Bisagni

Delft University of Technology, Faculty of Aerospace Engineering, Delft, 2629HS, Netherlands

Keywords: Fatigue, Delamination, S-N Diagram, Cohesive Zone Model

ABSTRACT

This paper focuses on a novel numerical formulation based on cohesive elements and S-N diagram to simulate fatigue-driven delamination in composite laminates. The constitutive model adopts a two-parameters heuristic equation, which coefficients are evaluated using an idealization of the S-N diagram rather than the more commonly used Paris law. The approach is implemented in the finite element code ABAQUS and validated with analysis on Double Cantilever Beam specimen. The numerical outcomes are compared with experimental data taken from literature showing the capability of the model in predicting the crack growth rate. The model is then applied to evaluate the fatigue delamination growth in a specimen similar to the Double Cantilever Beam but with reinforcement plates which force the delamination front to change its shape during the propagation. The results compared with experimental data taken from literature show the effectiveness of the approach in predicting the load-displacement curve and the delamination front shape and position at different load cycles.

1 INTRODUCTION

The estimation of the fatigue life of fibre-reinforced composite structures represents a key issue in the aerospace research, especially given the increasing trend in adopting composite materials for aeronautical primary structures. For this reason, it is essential to have effective numerical tools capable to take into account this phenomenon since the earliest stages of the design process.

Several methods can be adopted to experimentally characterize the fatigue behavior of a material or a structure. They can be divided in two main categories: phenomenological approaches based on the S-N curves and fracture mechanics methodologies based on the Fatigue Crack Growth (FCG) curves.

The S-N curve is the simplest and most common way to evaluate the fatigue life of a specimen. It represents the number of cycles that a material is able to sustain before failure at a given value of the applied stress. On the other hand, when dealing with crack propagation problem, approaches based on fracture mechanics are preferred because they provide information regarding the crack growth rate as a function of a fracture mechanics parameter, such as the stress intensity factor or the energy release rate. The crack propagation is usually described with the Paris law [1]:

$$\frac{da}{dN} = C(G)^m \tag{1}$$

where da is the crack extension measured during an increment of the number of cycles dN, G is the energy release rate and C and m are material parameters which depend on the stress ratio and mode-mixity.

In the last decades, several attempts have been made to incorporate the Paris law within a Finite Element (FE) analysis in order to numerically evaluate the fatigue crack propagation. The Virtual Crack Closure Technique (VCCT) has been employed by many authors to evaluate the energy release rate at the delamination front and then, using the Paris law, calculate the crack growth rate. However, this technique requires complex algorithms to track the crack front during the propagation and cannot be used for the simulation of damage initiation. Cohesive elements have gained considerable attention in the last years, because they are able to overcome some of these issues. Several authors have proposed cohesive formulations able to link the damage variable, which describes the stiffness degradation of the interface element, with the crack propagation rate defined by the Paris law. Some of

the earliest developed models make use of the length of the process zone to calculate the cohesive damage rate [2-3]. However, this value depends on different parameters, such as the mode-mixity, may change during the propagation of the damage and, in common structural problems, it is not a material properties but rather a structural characteristic. Although the estimation of the process zone length can be performed for specific load cases, it is not available an analytical expression to evaluate it for generic load conditions. Recently, some authors have attempted to solve this issue by proposing cohesive formulations which do not require the definition of the process zone length [4-5]. However, the Paris law coefficients depend on several factors, such as the mode-mixity, the stress ratio, the R-curve effects, and it seems that does not exist a single equation which can take into account all these aspects. To measure the influence of all these parameters an extremely large number of experimental tests would be required.

With the aim to overcome these issues, a novel fatigue cohesive formulation, based on the S-N diagram rather than on the Paris law, has been presented by Dávila in [6]. The starting point of the proposed model is the mixed-mode cohesive law developed by Turon et al. in [7]. The damage accumulated in one point is function of a two-parameter damage law which can be easily extracted from the S-N diagram. It is a purely local model which means that the damage in one point depends only on the history of the cyclic or on the tearing damage in that point. This formulation is here implemented inside the FE code ABAQUS and validated with experimental results of Double Cantilever Beam (DCB) specimens taken from literature and then it is used to analyze a specimen with a more complex geometry.

2 COHESIVE FATIGUE MODEL BASED ON THE S-N DIAGRAM

The S-N diagram describes the number of cycles required to reach the failure of a specimen with a given maximum stress and stress ratio ($R=\sigma_{min}/\sigma_{max}$).

In Fig. 1, the transverse tension fatigue life of unidirectional graphite/epoxy IM7/8552 is reported in a S-N diagram. The data are obtained from three-point bending and four-point bending tests at a stress ratio of 0.1 and the applied stress is normalized by the static strength (σ_c).

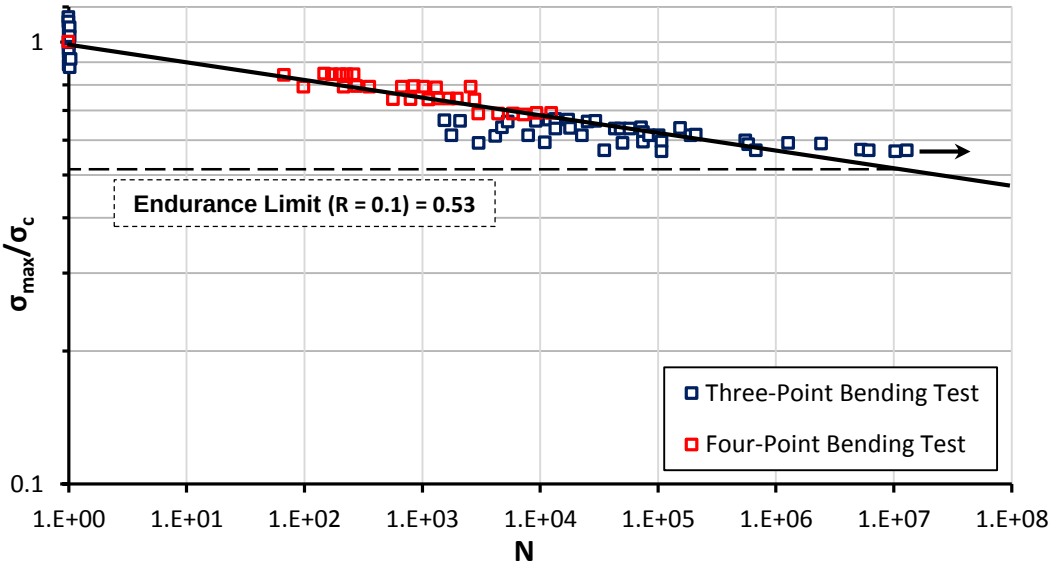

Figure 1: S-N diagram of matrix tensile failure IM7/8552 [8].

For composite materials the S-N diagram can be approximated with a straight line, while for metal or more ductile materials three lines are required. As it can be noted from Fig. 1, the entire diagram can be described by a single number, the endurance limit, defined as the maximum stress at which the specimen can sustain 10^7 load cycles without failure [9]. Several studies on different materials have demonstrated that the endurance limit of a specimen subjected to fully reversed loading ($R = -1$) can be well approximated as 1/3 of the tensile strength ($\sigma_e=\sigma_c/3$) [9-10]. At different stress ratios, the

endurance limit can be estimated using the Goodman diagram [10], which represents the combination of amplitude and limit stress corresponding to the failure of the specimen in a given number of cycles, 10^7 in the previous example. Considering a cyclic load oscillating between σ_{max} and σ_{min} the amplitude stress (σ^{amp}) and the mean stress (σ^{mean}) can be defined as follow:

$$\sigma^{amp} = \sigma_{\max}\frac{1-R}{2} \qquad \sigma^{mean} = \sigma_{\max}\frac{1-R}{2} \tag{2}$$

The Goodman diagram predicts a straight line connection between the endurance limit and the failure stress, given in equation (3) and shown in Fig. 2.

$$\sigma^{amp} = \sigma_e\left(1-\frac{\sigma^{mean}}{\sigma_c}\right) \tag{3}$$

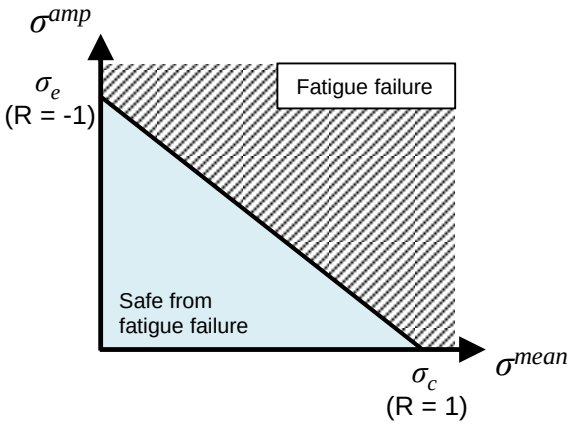

Figure 2: Goodman diagram.

Defining the endurance limit as the maximum stress for a given stress ratio ($\sigma_{eR}=\sigma_{max}$) that fulfill the conditions of equation (3), and substituting equation (2) into equation (3), the following expression is obtained:

$$\sigma_{eR}\left(\frac{1-R}{2}+\frac{1+R}{2}\frac{\sigma_e}{\sigma_c}\right)=\sigma_e \tag{4}$$

Considering the assumption that the endurance limit for R = -1 is 1/3 of the strength, an equation for the endurance limit as a function of the stress ratio is achieved:

$$\sigma_{eR} = \frac{\sigma_c}{2-R} \tag{5}$$

The model proposed by Dávila is based on equation (5) and on the hypothesis of linearity of the S-N diagram to evaluate the fatigue behavior of any material subjected to different stress ratios. The proposed cohesive law is derived from the mixed-mode formulation developed by Turon et al. in [7] for the tearing damage with the addition of a procedure to track the evolution of fatigue damage.

Considering an unnotched bar subjected to a sinusoidal stress oscillating between σ_{min} and σ_{max}, the evolution of the traction within the material follows the path illustrated in Fig. 3.

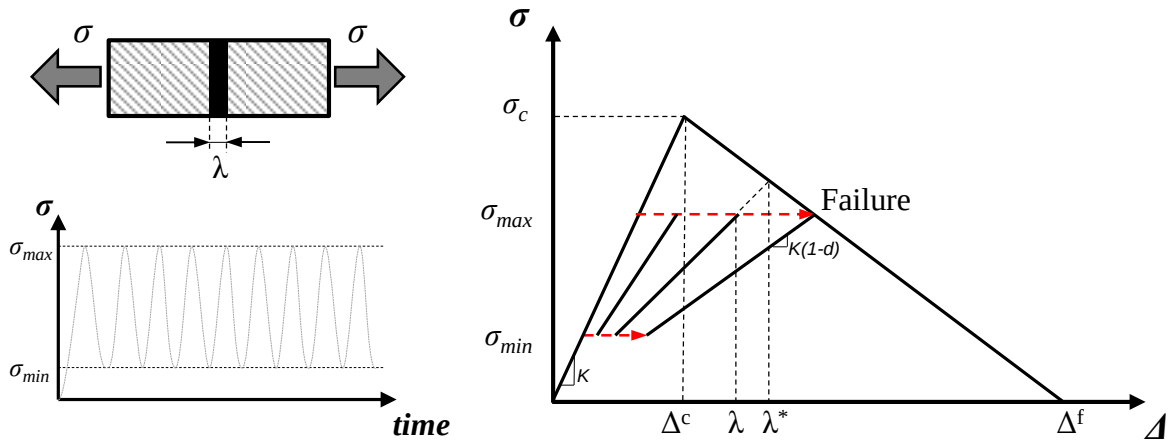

Figure 3: Cohesive fatigue constitutive model.

If σ_{max} is below the strength of the material σ_c, at each cycle the displacement associated with the maximum stress increases, up to the point in which the material is not able to sustain anymore the load, leading to an unstable failure. In this process, to describe the evolution of the damage within the cohesive element, Dávila proposed the following two-parameters heuristic equation:

$$\frac{dD}{dN} = (D+\gamma)\left(\frac{\lambda}{\lambda^*}\right)^{\beta} \tag{6}$$

where D is the damage norm, defined as:

$$D = \frac{\lambda^* - \Delta^c}{\Delta^f - \Delta^c} \tag{7}$$

and the ratio between the displacements at any point is defined, referring to Fig. 3, as:

$$\frac{\lambda}{\lambda^*} = \frac{\sigma_{\max}}{(1-D)\sigma_c} \tag{8}$$

The damage norm is independent to the cohesive stiffness and can be related to the damage variable (d), usually adopted to represent the loss of stiffness in cohesive elements, with the equation (9):

$$1-d = \frac{\lambda^* - \Delta^f D}{\lambda^*} \tag{9}$$

The total number of cycles at failure (N^f) can be evaluated integrating the equation (6) between $D = 0$ and $D = D^F$, which is the value of the damage norm at the failure.

$$N^f = \left(\frac{\sigma_c}{\sigma_{\max}}\right)^{\beta} \int_0^{D^F} \frac{(1-D)^{-\beta}}{D+\gamma} dD \tag{10}$$

where:

$$D^F = 1 - \frac{\sigma_{\max}}{\sigma_c} \tag{11}$$

The coefficient β and γ in equation (6), depend on the stress ratio and are evaluated fitting the S-N diagram. In order to fit the curve, which for composite materials is a straight line, two points are needed. The first point corresponds to the strength of the material, arbitrarily set to 2 cycles, while the second point is the endurance of the material (σ_{eR}) after 10^7 cycles, evaluated with equation (5). These

two conditions are used in equation (10) to obtain a nonlinear system of two equations and two variables which can be numerically solved to find the value of the coefficients.

The cohesive damage model is implemented in the FE code ABAQUS by means of a User Material Subroutine (UMAT) [11], which is called at each integration point during each load increment of the non-linear analysis. The analysis is performed with the "envelope load method", in which, instead of simulating the whole variation of the load for each cycle, only the maximum load of a single cycle is applied and kept constant. The load variation is taking into account inside the cohesive constitutive model.

3 NUMERICAL VALIDATION

The S-N based approach is validated performing numerical simulations on a DCB specimen which is the standard test to characterize quasi-static delamination propagation in pure mode I, but it is also used for fatigue load conditions. The DCB specimen considered in this work has been experimentally tested in [12] and consists of a rectangular plate 178 mm long and 25.4 mm wide, manufactured using 24 unidirectional layers of graphite/epoxy IM7/8552. The numerical model is discretized with continuum shell elements (SC8R) and zero-thickness cohesive elements. To accurately represent the cohesive process zone, an element length of 0.04 mm is adopted in the propagation areas. However, to reduce the computational effort, only 1 mm of the width is modeled and the reaction force is scaled by the actual width of the specimen. The FE model and the material properties are shown in Fig. 4 and Table 1, respectively.

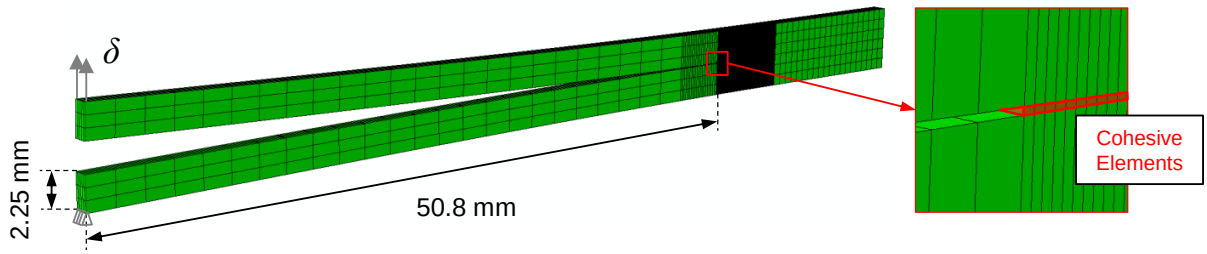

Figure 4: DCB FE model.

Lamina properties			Interface properties		
$\mathbf{E_1}$	[MPa]	146671	$\mathbf{G_{1C}}$	[kJ/m^2]	0.240
$\mathbf{E_2 = E_3}$	[MPa]	8703	$\mathbf{G_{2C}}$	[kJ/m^2]	0.739
$\mathbf{G_{12} = G_{13}}$	[MPa]	5164	$\boldsymbol{\eta}$		2.1
$\mathbf{G_{23}}$	[MPa]	3001	$\boldsymbol{\sigma_c}$	[MPa]	80.1
$\boldsymbol{\nu_{12} = \nu_{13}}$		0.32	$\boldsymbol{\tau_c}$	[MPa]	97.6
$\boldsymbol{\nu_{23}}$		0.45			

Table 1: IM7/8552 material properties.

The analysis is conducted under displacement control conditions and divided in two steps: in the first quasi-static step, the displacement is increased up to the maximum value of the fatigue cycle, then, in the second step, it is kept constant and the fatigue algorithm is activated. A stress ratio of 0.1 is used in the constitutive model to reproduce the experimental tests. The value of coefficients β and γ evaluated according to equation (10) are reported in Table 2.

R	β	γ
0.1	23.649	0.001911

Table 2: Fatigue damage model coefficients.

The length of the delamination and therefore the crack growth rate can be evaluated using the equations derived from the corrected beam theory [13]. These equations allow to calculate the crack length and the energy release rate from the compliance of the specimen (C=δ/F), which can be easily evaluated extracting the reaction force from the numerical analysis, since the displacement is constant.

The expressions for the calculation of the crack length and of the energy release rate are reported in equation (12):

$$a = \left(\frac{3}{2}CEI\right)^{1/3} - \chi h \qquad G_I = \frac{(a+\chi h)^2}{bEI}F^2 \tag{12}$$

where b is the width of the specimen, h is the thickness of each arm and:

$$\chi = \sqrt{\frac{E_1}{11G_{13}}\left[3-2\left(\frac{\Gamma}{1+\Gamma}\right)^2\right]} \qquad \Gamma = 1.18\frac{\sqrt{E_1E_2}}{G_{13}} \qquad EI = E_1\frac{bh^3}{12} \tag{13}$$

Analyses at different values of the maximum displacement are performed and the results in terms of crack growth rate as function of the energy release rate are reported in Fig. 5 and compared with the experimental data from [12].

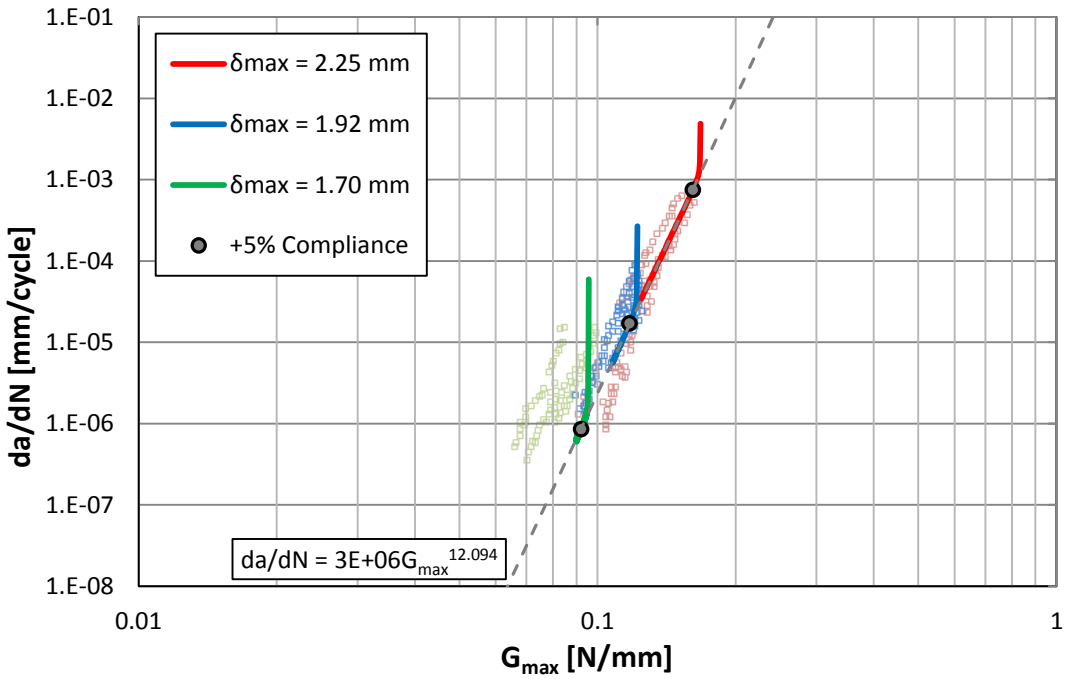

Figure 5: Comparison between numerical and experimental crack growth rate for a DCB at different applied displacements.

The point in which the compliance of the specimen increases by 5% corresponds to a growth in crack length of 0.9 mm which is usually considered as the delamination propagation onset. As it can be observed in Fig. 5, for all the simulations, the crack growth rate is high at beginning, but rapidly decreases and after the beginning of the propagation it starts to follow a straight line. This line clearly represents the typical Paris law equation which agrees well with the data obtained from experimental tests at the same maximum applied displacements.

As demonstrated by Dávila in [6] an even better correlation between the numerical and experimental data can be obtained taking into account the effect of fiber bridging and representing the R-curve of the material with a superposition of two cohesive laws.

4 NUMERICAL APPLICATION

The fatigue constitutive model adopted in this work is employed to simulate fatigue crack propagation in a more complex specimen, in which the crack front does not evolve as a straight line. The benchmark test proposed by Carreras et al. in [14], although it is simple in terms of geometry, exhibits a relatively complex behavior in terms of delamination propagation. The specimen is called reinforced DCB, because it is similar to a DCB but with two reinforcement plates bonded on top and bottom of the two arms. The reinforcements do not extend over the entire length and width of the specimen, forcing the delamination front to curve during the propagation. The geometrical characteristics and the properties of the material system are reported in Fig. 6 and Table 3.

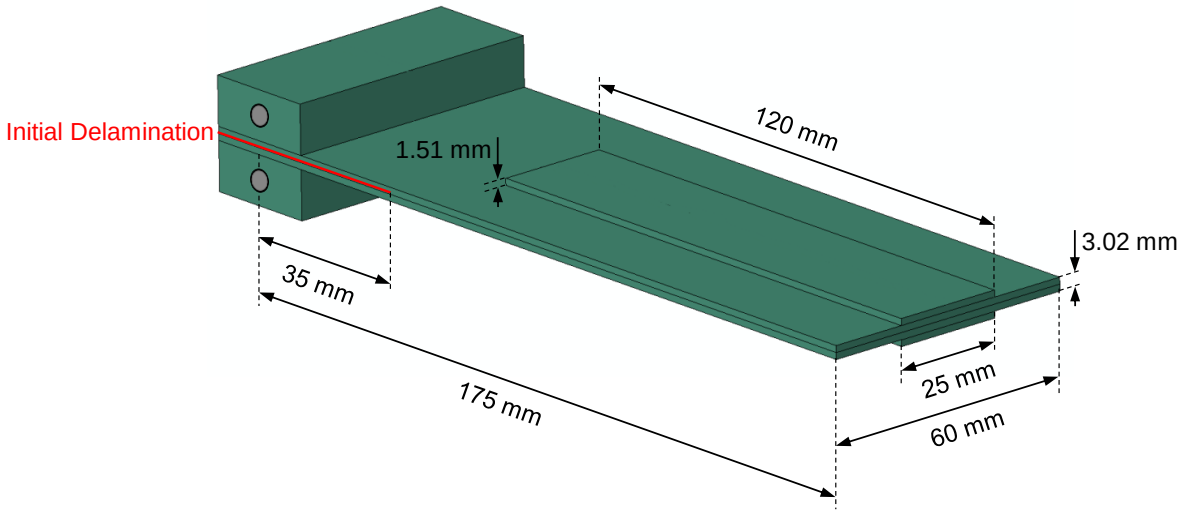

Figure 6: Reinforced DCB geometrical dimensions.

Lamina properties			Interface properties		
E_1	[MPa]	154000	G_{1C}	[kJ/m^2]	0.305
$E_2 = E_3$	[MPa]	8500	G_{2C}	[kJ/m^2]	2.77
$G_{12} = G_{13}$	[MPa]	4200	η		2
G_{23}	[MPa]	3036	σ_c	[MPa]	10
$\nu_{12} = \nu_{13}$		0.35	τ_c	[MPa]	31.62
ν_{23}		0.4			

Table 3: Material properties adopted in the numerical simulation [15].

Since the specimen is symmetric in terms of geometry, material and boundary conditions, only half of the structure is discretized to reduce the computational resources. One layer of SC8R elements with an element length of approximately 2 mm is adopted to represent the arms and the reinforcement plates, while a very fine discretization is used in the area potentially interested by the propagation of the delamination, with an elements length of 0.05 mm.

The numerical analysis is performed under displacement controlled conditions and divided in two steps. In the first quasi-static step, the displacement of the top arm is increased up to the maximum opening displacement of 5 mm, and only the static damage is taking into account. In the second step, the displacement is kept constant and the fatigue damage is evaluated considering a load ratio of 0.1, to replicate the experimental test, and the same model parameters used for the DCB, reported in Table 2.

In Fig. 7, the FE model is shown together with the boundary conditions.

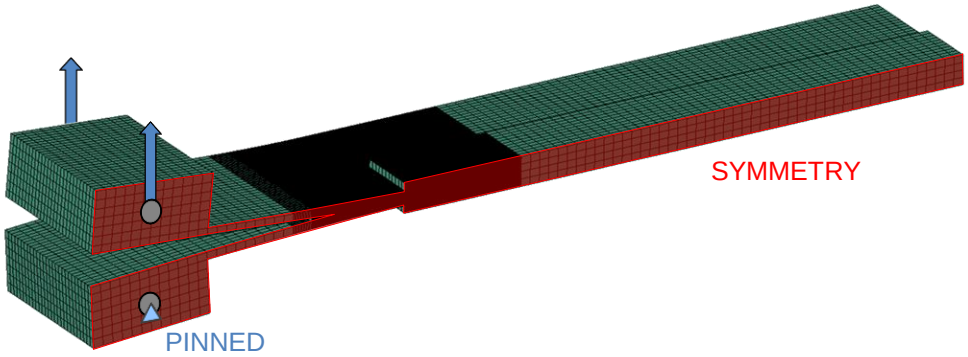

Figure 7: Reinforced DCB FE model.

The reaction force as function of the applied displacement is compared in Fig. 8 with the experimental data from three different specimens.

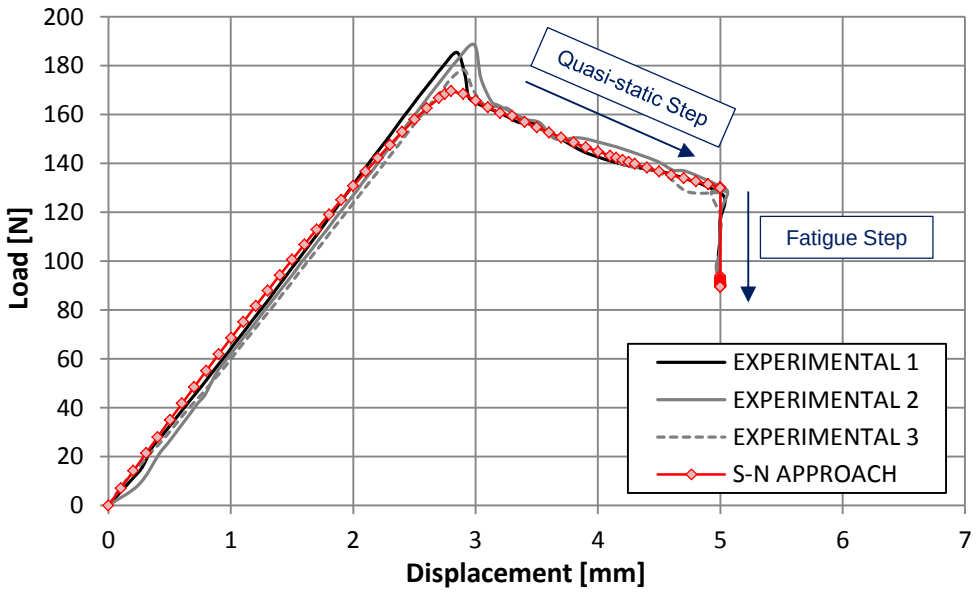

Figure 8: Load-displacement curves of the reinforced DCB.

The force increases up to the maximum value at a displacement of around 3 mm, then the delamination starts to propagate and the load decreases.

When the displacement reaches the final value of 5 mm, the fatigue analysis starts and the stiffness decreases due to the propagation of the delamination. The agreement of the numerical results with the experimental data is excellent throughout the quasi-static and the fatigue step except for a slightly underestimation of the maximum load.

The evolution of the delamination front can be seen in Fig. 9, where the cohesive process zone is reported and compared to the crack front measured during the experimental test at different load cycles.

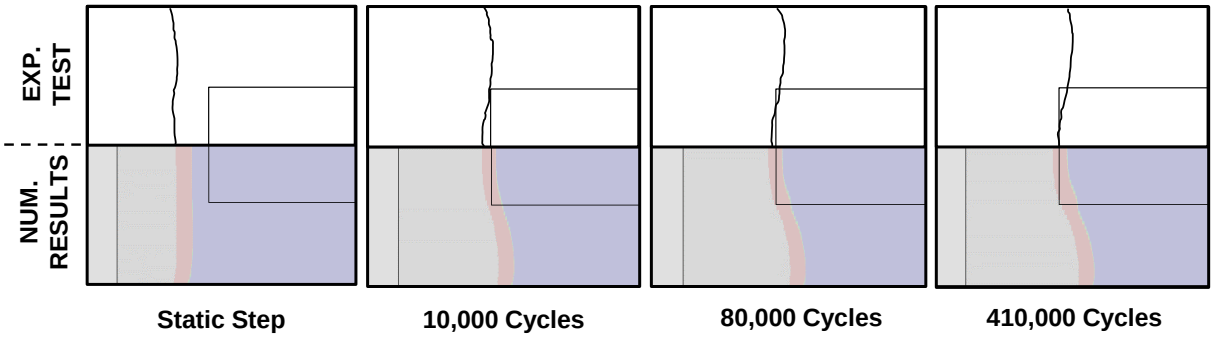

Figure 9: Comparison between numerical and experimental delamination front at different load cycles.

The delamination growth, as expected, is limited in the center by the presence of the reinforcements, while on the edges the crack front assumes a rounded shape. There is a good agreement between numerical and experimental data in terms of delamination front position and shape, although the numerical analysis slightly overestimates the propagation on the edge of the panel.

5 CONCLUSIONS

A cohesive formulation for the simulation of delamination propagation in composite laminates has been investigated. The constitutive model is based on a two-parameter heuristic equation where the coefficients are determined from the S-N diagram rather than the more commonly used Paris law. The fatigue model has been adopted to analyze a pure mode I delamination propagation in a DCB specimen. The crack growth rates predicted by the numerical analysis have shown an excellent correlation with the experimental data and in particular they are aligned along a straight line, similar to a Paris law.

The same approach has been adopted to simulate fatigue-driven delamination in a more complex specimen, similar to the DCB but with reinforcements bonded on the two arms. The presence of the reinforcements delays the propagation of the delamination in the center of the specimen and forces the crack front to change its shape which evolves from a straight line into a complex curved shape. The comparison with the experimental results of three different specimens have shown a good agreement in terms of load-displacement curve and delamination front shape and position at different cycles.

ACKNOWLEDGEMENTS

The first author has received funding from the European Union's Horizon 2020 research and innovation programme under the Marie Skłodowska-Curie grant agreement No 707404. The authors would like to thank Dr. Carlos G. Dávila from NASA Langley Research Center for having introduced to the research presented in this work.

REFERENCES

[1] P.C. Paris, M.P. Gomez and W.E. Anderson, A rational analytic theory of fatigue, *The Trend in Engineering*, **13(1)**, 1961, pp 9-14.

[2] A. Turon, J. Costa, P.P. Camanho and C.G. Dávila, Simulation of delamination in composites under high-cycle fatigue, *Composites Part A: Applied Science and Manufacturing*, **38(11)**, 2007, pp. 2270-2282 (doi: 10.1016/j.compositesa.2006.11.009).

[3] A. Pirondi and F. Moroni, A progressive damage model for the prediction of fatigue crack growth in bonded joints, *The Journal of Adhesion*, **86(5–6)**, 2010, pp. 501-521 (doi: 10.1080/00218464.2010.484305).

[4] L.O. Voormeeren, F.P. van der Meer, J. Maljaars and L.J. Sluys, A new method for fatigue life prediction based on the thick level set approach, *Engineering Fracture Mechanics*, **182**, 2017, pp. 449-466 (doi: 10.1016/j.engfracmech.2017.05.007).

[5] B.L.V. Bak, A. Turon, E. Lindgaard and E. Lund, A simulation method for high-cycle fatigue-driven delamination using a cohesive zone model, *International Journal of Numerical Methods in Engineering*, **106**, 2016, pp. 163-191 (doi: 10.1002/nme.5117).

[6] C.G. Dávila, From S-N to the Paris law with a new mixed-mode cohesive fatigue model, NASA/TP–2018-219838, 2018.

[7] A. Turon, E.V. González, C. Sarrado, G. Guillamet and P. Maimí, Accurate simulation of delamination under mixed-mode loading using a cohesive model with a mode-dependent penalty stiffness, *Composite Structures*, **184**, 2018, pp. 506-511 (doi: 10.1016/j.compstruct.2017.10.017).

[8] T.K. O'Brien, A.D. Chawan, R. Krueger I.L. and Paris, Transverse tension fatigue life characterization through flexure testing of composite materials, *International Journal of Fatigue*, **24(2-4)**, 2002, pp. 127-145 (doi: 10.1016/S0142-1123(01)00104-9).

[9] N.A Fleck, K.J. Kang and M.F. Ashby, Overview No. 112: The cyclic properties of engineering materials, *Acta Metallurgica et Materialia*, **42(2)**, 1994, pp. 365-381 (doi: 10.1016/0956-7151(94)90493-6).

[10] J. Goodman, *Mechanics Applied to Engineering*, Longmans, Green and Co., London, UK, 1899.

[11] Abaqus Analysis Guide. Dassault Systemes. 2017.

[12] G.B. Murri, Evaluation of delamination onset and growth characterization methods under mode I fatigue loading, Technical Report NASA/TM–2013-217966, 2013.

[13] J.R. Reeder, K. Demarco and K.S. Whitley, The use of doubler reinforcement in delamination toughness testing, *Composites Part A: Applied Science and Manufacturing*, **35(11)**, 2004, pp. 1337-1344 (doi: 10.1016/j.compositesa.2004.02.021).

[14] L. Carreras, J. Renart, A. Turon, J. Costa, B.L.V. Bak, E. Lindgaard, F. Martin de la Escalera and Y. Essa, A benchmark test for validating 3D simulation methods for delamination growth under quasi-static and fatigue loading, *Composite Structures*, **210**, 2019 pp. 932–941 (doi: 10.1016/j.compstruct.2018.12.008).

[15] L. Carreras, B.L.V. Bak, A. Turon, J. Renart and E. Lindgaardb, Point-wise evaluation of the growth driving direction for arbitrarily shaped delamination fronts using cohesive elements, *European Journal of Mechanics – A/Solids*, **72**, 2018, pp. 464–482 (doi: 10.1016/j.euromechsol.2018.05.006)